

# Ubiquitous nematic Dirac semimetal emerging from interacting quadratic band touching system

Hongyu Lu

Department of Physics, University of Hong Kong



## Introduction

Quadratic band touching (QBT) points are widely observed in 2D and 3D materials, including bilayer graphene and Luttinger semimetals, and attract significant attention from theory to experiment. However, even in its simplest form, the 2D checkerboard lattice QBT model, the phase diagram characterized by temperature and interaction strength still remains unknown beyond the weak-coupling regime. Intense debates persist regarding the existence of various interaction-driven insulating states in this system. To address these uncertainties, we employ thermal tensor network simulations, specifically XTRG and  $\tan$ TRG along with DMRG calculations to provide a comprehensive finite-temperature phase diagram for this model and shed light on previous ambiguities. Notably, our findings reveal the emergence of a robust bond-nematic Dirac semimetal (BNDS) phase with distinct thermodynamic properties that set it apart from the nematic insulating state and other symmetry broken states. This previously overlooked feature is found to be ubiquitous in interacting QBT systems. We also discuss the implications of these results for experimental systems such as bilayer graphene and iridate compounds.

## Spinless fermion model in a checkerboard lattice

### The QBT model

$$\begin{aligned}
 H = & \sum_{\mathbf{r}} [t \sum_{\gamma} c_{\mathbf{r},B}^{\dagger} c_{\mathbf{r}+\gamma,A} + \text{h.c.}] \quad (\text{NN}) \\
 & + t' \sum_{\lambda,i} (\eta_{\lambda} \epsilon_i) c_{\mathbf{r},\lambda}^{\dagger} c_{\mathbf{r}+\mathbf{a}_i,\lambda} + \text{h.c.} \quad (\text{NNN}) \\
 & + V_1 \sum_{\gamma} (n_{\mathbf{r},B} - \frac{1}{2})(n_{\mathbf{r}+\gamma,A} - \frac{1}{2}) \quad (\text{NN}) \\
 & + V_2 \sum_{\lambda,i} (n_{\mathbf{r},\lambda} - \frac{1}{2})(n_{\mathbf{r}+\mathbf{a}_i,\lambda} - \frac{1}{2}), \quad (\text{NNN})
 \end{aligned} \quad (1)$$

with  $\gamma \in \{\mathbf{0}, \mathbf{a}_1, \mathbf{a}_2, \mathbf{a}_1 + \mathbf{a}_2\}$ ,  $\lambda \in \{A, B\}$  being the sublattice index,  $\{\eta_A = 1, \eta_B = -1\}$  and  $\{\epsilon_1 = 1, \epsilon_2 = -1\}$ . We fix  $t = -1$  and  $t' = -0.5$  and consider both the repulsive NN and NNN density-density interactions.

## Order parameters / Structure factors

In our simulations, we use the following order parameters or structure factors, identifying different phases.

- **QAH structure factor** with  $\mathcal{J}_{\text{QAH}} \equiv \frac{1}{N_b} \sum_{\langle i,j \rangle} \epsilon_{i,j} \langle \mathcal{C}_{ij} \mathcal{C}_{i_0 j_0} \rangle$ , where the summation is over NN bonds in the bulk with  $N_b$  being the total number of bonds and  $\epsilon_{i,j} = \pm 1$  characterizing the orientation of the current  $\mathcal{C}_{ij} \equiv (c_i^{\dagger} c_j - c_j^{\dagger} c_i)$ ;
  - **Bond-nematic order** with  $\Delta_{\text{bond}} \equiv |\langle c_{\mathbf{r},\lambda}^{\dagger} c_{\mathbf{r}+\mathbf{a}_2,\lambda} \rangle| - |\langle c_{\mathbf{r},\lambda}^{\dagger} c_{\mathbf{r}+\mathbf{a}_1,\lambda} \rangle|$ , which measures the difference in NNN hopping amplitudes along the vertical ( $\mathbf{a}_2$ ) and horizontal ( $\mathbf{a}_1$ ) directions;
  - **Site-nematic order** with  $\delta_{\text{site}} \equiv \langle n_B - n_A \rangle$ , which quantifies the difference of electron density at 'A' and 'B' sublattices;
  - **Stripe structure factor** with  $\mathcal{S}_{\text{stripe}} \equiv \frac{1}{N} \sum_i e^{-i\vec{k} \cdot \vec{r}_i} (\langle \hat{n}_i \hat{n}_0 \rangle - \langle \hat{n}_i \rangle \langle \hat{n}_0 \rangle)$ , where  $\vec{k} = (\pm \frac{\sqrt{2}\pi}{2}, \mp \frac{\sqrt{2}\pi}{2})$ .
- Patterns of the 4 phases are shown in Fig.1.

## Results

### Phase Diagram

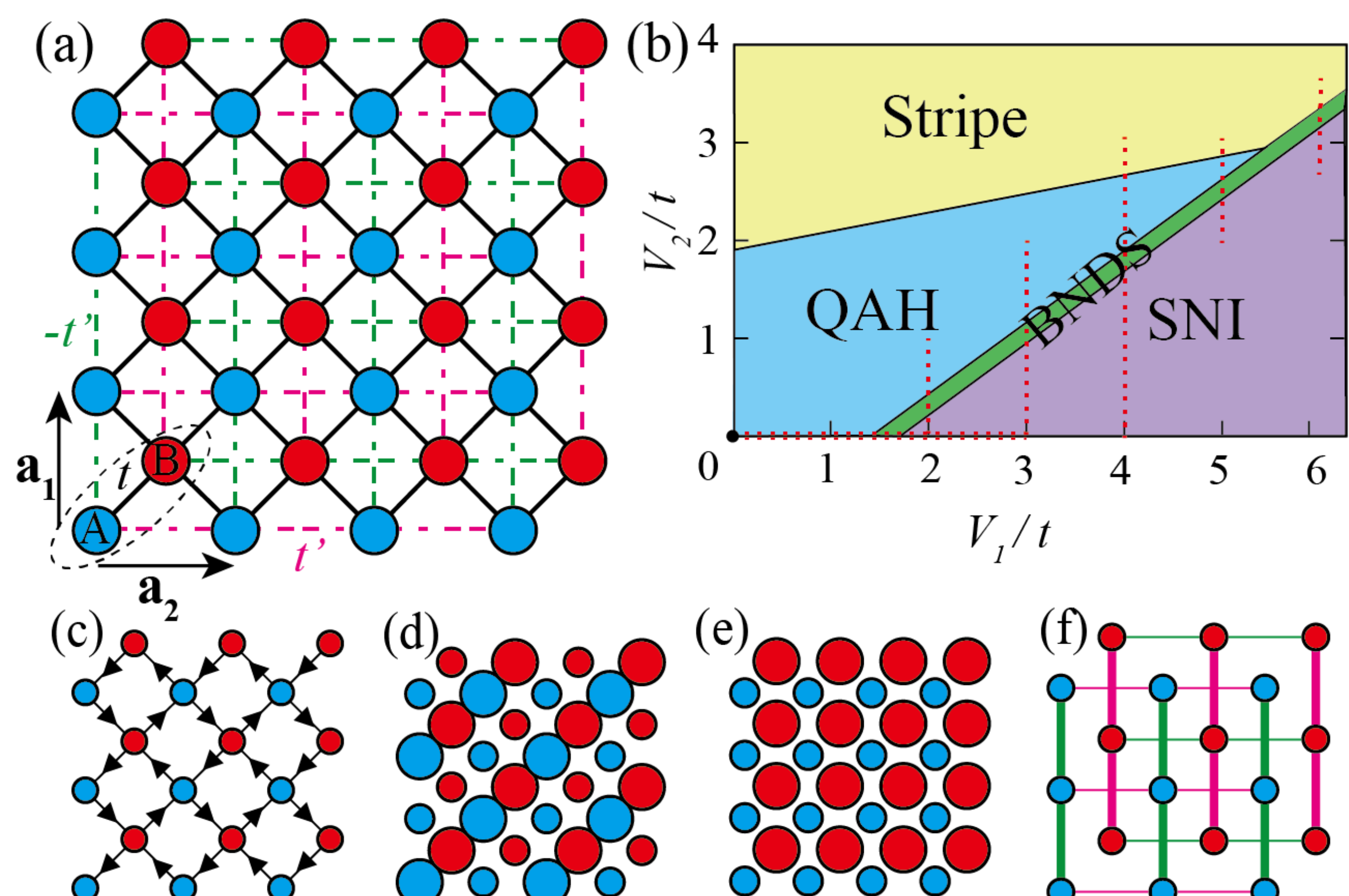


Fig 1: (a) The checkerboard lattice with blue (red) dots denoting the A (B) sublattices. (b) The comprehensive ground-state phase diagram. The QBT is denoted by the black dot at the origin, while the red dotted lines represent the paths of simulations. (c)-(f) The real-space signature of the Quantum Anomalous Hall (QAH), Stripe insulator, site-nematic insulator (SNI), and BNDS phases, respectively. The QAH phase is depicted with arrows indicating the loop currents. In the Stripe and SNI phases, large (small) dots represent high (low) electron density. In the BNDS phase, the thickness of the bonds corresponds to the absolute value of the hopping amplitude.

## Results

### $T - V$ phase diagram

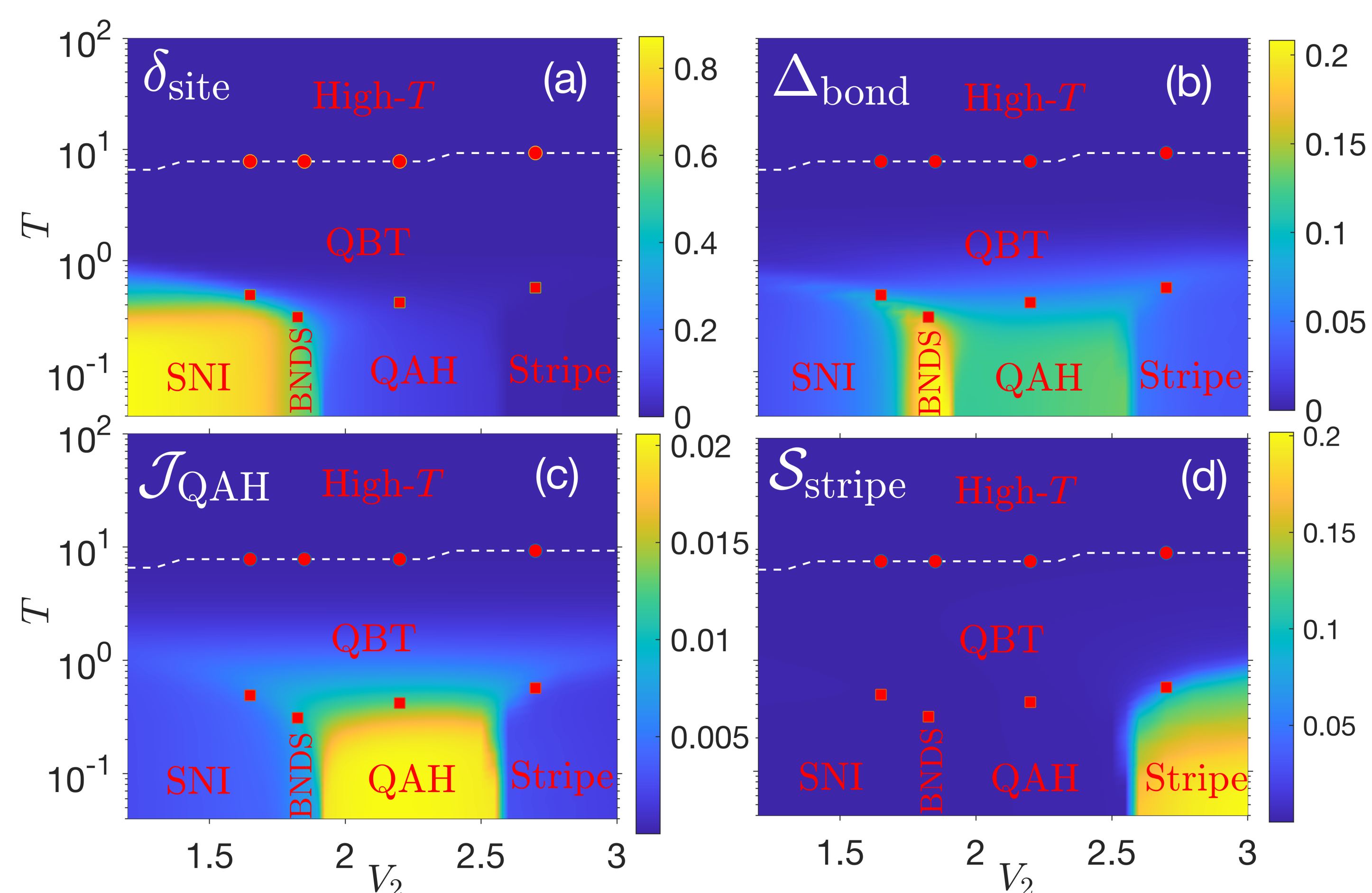


Fig 2: The  $T - V_2$  phase diagrams at  $V_1 = 4$ . Plots show (a) the SNI order parameter, (b) BNDS order parameter, (c) QAH structure factor, and (d) stripe structure factor. The white dashed lines indicate the boundaries between the high-temperature thermal metallic regime and the intermediate-temperature QBT regime, identified using the red circles, which represent the crossover temperature between the high- $T$  and QBT regimes. The red squares denote the transition temperature between the QBT regime to the low-temperature symmetry-breaking phases.

### Thermodynamic characteristics

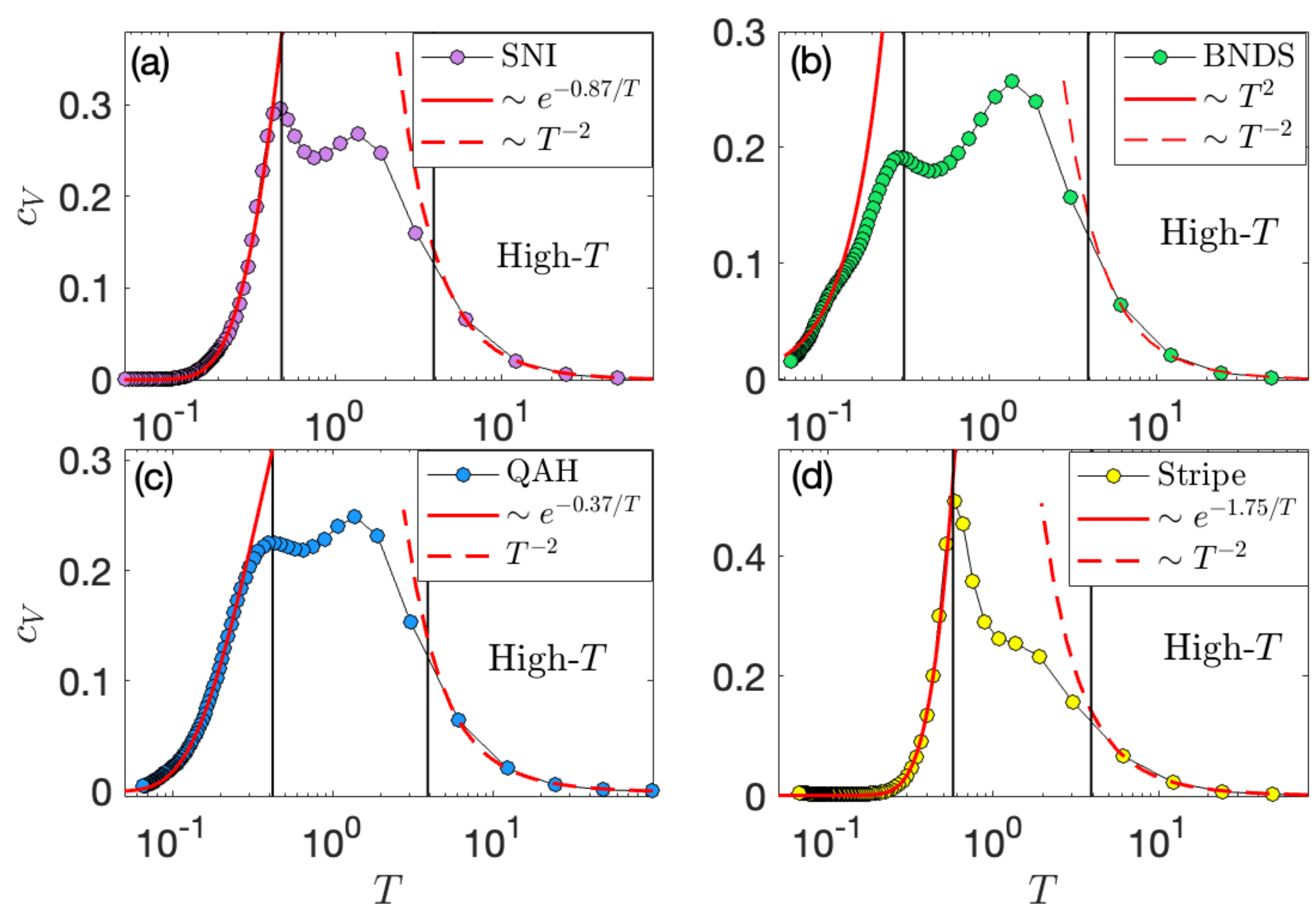


Fig 3: The specific heat along the cuts in Fig. 2 as a function of temperature  $T$ . With fixed  $V_1 = 4$ , (a) represent SNI at  $V_2 = 1.65$ , (b) represent BNDS at  $V_2 = 1.85$ , (c) represent QAH at  $V_2 = 2.2$ , (d) represent Stripe at  $V_2 = 2.7$ . The separation temperature between the low-temperature, intermediate, and high-temperature regimes is indicated by the black solid lines. The  $C_V \sim T^2$  for BNDS at low temperature is distinctively different from the  $C_V \sim \exp(-\Delta/T)$  for the three other phases.

### BNDS in large- $V$ region

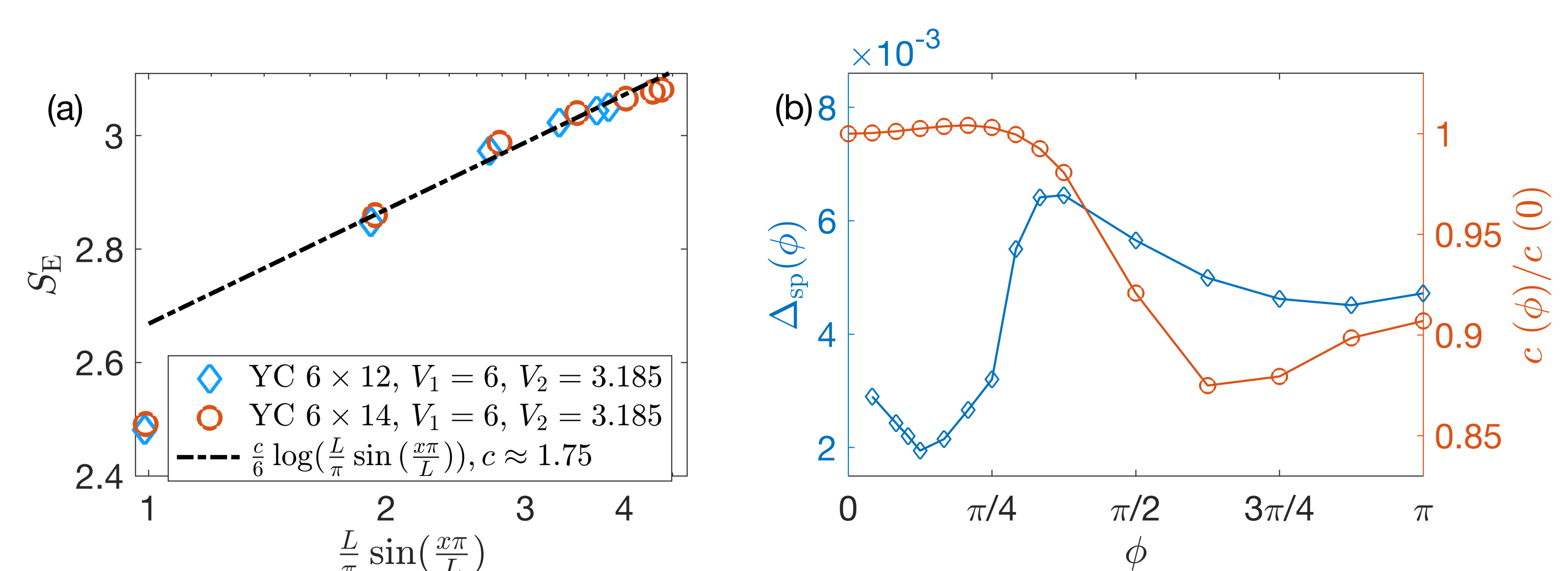


Fig 4: (a) Entanglement entropy in BNDS phase ( $V_1 = 6$ ,  $V_2 = 3.185$ , and  $D = 4096$ ), with log-scale horizontal axis. (b) With twisted boundary conditions in BNDS, by inserting flux  $\phi$ , the single-particle gap  $\Delta_{\text{sp}}(\phi)$  (by extrapolating the ground-state energy at half-filling sector and lowest energy in the single-particle-excited sector), and fitted central charge (fitting the entanglement entropy as a function of the cylinder length to the universal scaling function  $S_E(x) = \frac{c}{6} \log(\frac{L}{\pi} \sin(\frac{x\pi}{L}))$ ) compared with that of no flux are shown. Corresponding shift of momenta grids is  $\phi/L_y$ .

## Conclusion

- We find the interaction-driven BNDS ubiquitously exist between SNI and the other interaction-driven insulating states in the checkerboard lattice QBT system, and we provide the complete ground state and finite-temperature phase diagram with repulsive interactions, which solves the previous debates in this system.
- We find the transition between BNDS and SNI in the phase diagram is similar to the liquid-gas transition and provide the numerical results of the thermodynamic characteristics, in that the BNDS state is characterized by  $C_V \sim T^2$  of emergent Dirac cones from interacting QBT systems, distinctively different from the exponential form in other phases.

## References

HYL, Kai Sun, Zi-Yang Meng, and Bin-Bin Chen. Ubiquitous nematic Dirac semimetal emerging from interacting quadratic band touching system. arXiv: 2305.17189.